mater.scichina.com link.springer.com

Published online 25 December 2023 | https://doi.org/10.1007/s40843-023-2691-9
Sci China Mater 2024, 67(1): 242–250

Photothermal conversion mechanism of the dibenzotetrathiafulvalene-tetracyanobenzene cocrystal based on the transitions between the ground and excited states

Siyao Fu[1], Dan He[3] and Xiaotao Zhang[2*]

ABSTRACT **Organic cocrystals have been bringing hope and vitality into several fields, such as photothermal imaging, biological application, and seawater desalination, owing to their photothermal conversion property. However, their mechanism of photothermal conversion is particularly lacking detailed and in-depth theoretical research. In this study, time-dependent density functional theory was used to explore the excitation and deexcitation processes and explain the reason for the higher photothermal conversion efficiency of dibenzotetrathiafulvalene-tetracyanobenzene (DBTTF-TCNB) cocrystal than its component single crystals. The results reveal that the great proportion of high excited states promotes the occurrence of the nonradiative transition. Based on the result of the charge transfer between the electron-donating group and the electron-withdrawing group in the DBTTF-TCNB cocrystal, we found that the electron-withdrawing competition between the donor and acceptor might promote the photothermal conversion. Certainly, the electron-donating group in the cocrystal structure is also crucial. These results may offer some guidance for the design of photothermal conversion cocrystals. The orbital contribution and electron density difference further confirm our conclusion. Therefore, our research could provide the basis for applications of photothermal cocrystals in innovative fields from the perspective of quantum chemistry.**

Keywords: organic cocrystal, photothermal conversion, nonradiative transition, quantum chemistry calculation

INTRODUCTION

Organic cocrystals, which are based on the charge transfer (CT) interaction between the electron donor and the electron acceptor [1–5], have recently been used innovatively in many fields such as photothermal imaging [6–9], biological application [6,10–15], and seawater desalination [6,16–18], owing to their unique photothermal conversion (PTC) property. The PTC property brings new hope and vitality to the practical applications of organic cocrystals [6]. Of course, there is the question of—why organic cocrystals have better photothermal properties than organic single crystals. For this question, some experimental studies on photothermal cocrystals [6–8,19–21] and theoretical calculations on the de-excitations of excited states [22–25] have presented several explanations, which mainly include the inhibition of radiative transition and promotion of nonradiative transition.

Generally, fluorescence emission and phosphorescence emission are radiative transitions, whereas vibrational relaxation, internal conversion, and intersystem crossing are nonradiative transitions [26,27]. For PTC, many studies put it down to more occurrences of vibrational relaxation, internal conversion, or intersystem crossing [6–8,21]. However, there is little research on the process of nonradiative transition. Therefore, we are interested to know what happens in this process.

Recently, density functional theory (DFT) [28] has achieved unprecedented development owing to the improvement of computing power and theoretical knowledge [29–32]. Several quantum chemists apply the DFT to solve various problems that cannot be solved using experimental methods [30,31,33]. Cocrystal formation is mostly attributed to the CT between the donor and the acceptor [1–5]. The CT is significant; hence, substantial attention is placed on the CT processes between the ground and excited states of the organic cocrystal system.

Briefly, we introduce two vital rules, namely, Jablonski diagram [34] and Kasha's rule [35]. Jablonski first described, in the form of energy level, the physical process of a molecule in which the energy is dissipated back to the ground state after the absorption of a photon [34]. Kasha's rule indicates that the emitting level of a given multiplicity is the lowest excited level of that multiplicity [35]. Herein, the two theories were applied for the analysis of the transitions between the ground and excited states.

Combining both theories, a concise schematic in Fig. 1a vividly and clearly explains our theoretical basis. In Fig. 1a, when the system absorbs a photon, several electrons are excited to higher states—different excited states. Based on Kasha's rule, only the first excited state, which is S_1 state, can release energy in the form of a photon. Other excited states can only release energy by nonradiative transition to S_1 state first and then go on releasing energy by photon emission. For this reason, we mainly

[1] Key Laboratory of Organic Integrated Circuits, Ministry of Education & Tianjin Key Laboratory of Molecular Optoelectronic Sciences, Department of Chemistry, School of Science, Tianjin University, Tianjin 300072, China
[2] Key Laboratory of Organic Integrated Circuits, Ministry of Education & Tianjin Key Laboratory of Molecular Optoelectronic Sciences, Department of Chemistry, Institute of Molecular Aggregation Science, Tianjin University, Tianjin 300072, China
[3] College of Chemistry and Chemical Engineering, Central South University, Changsha 410083, China
* Corresponding author (email: zhangxt@tju.edu.cn)

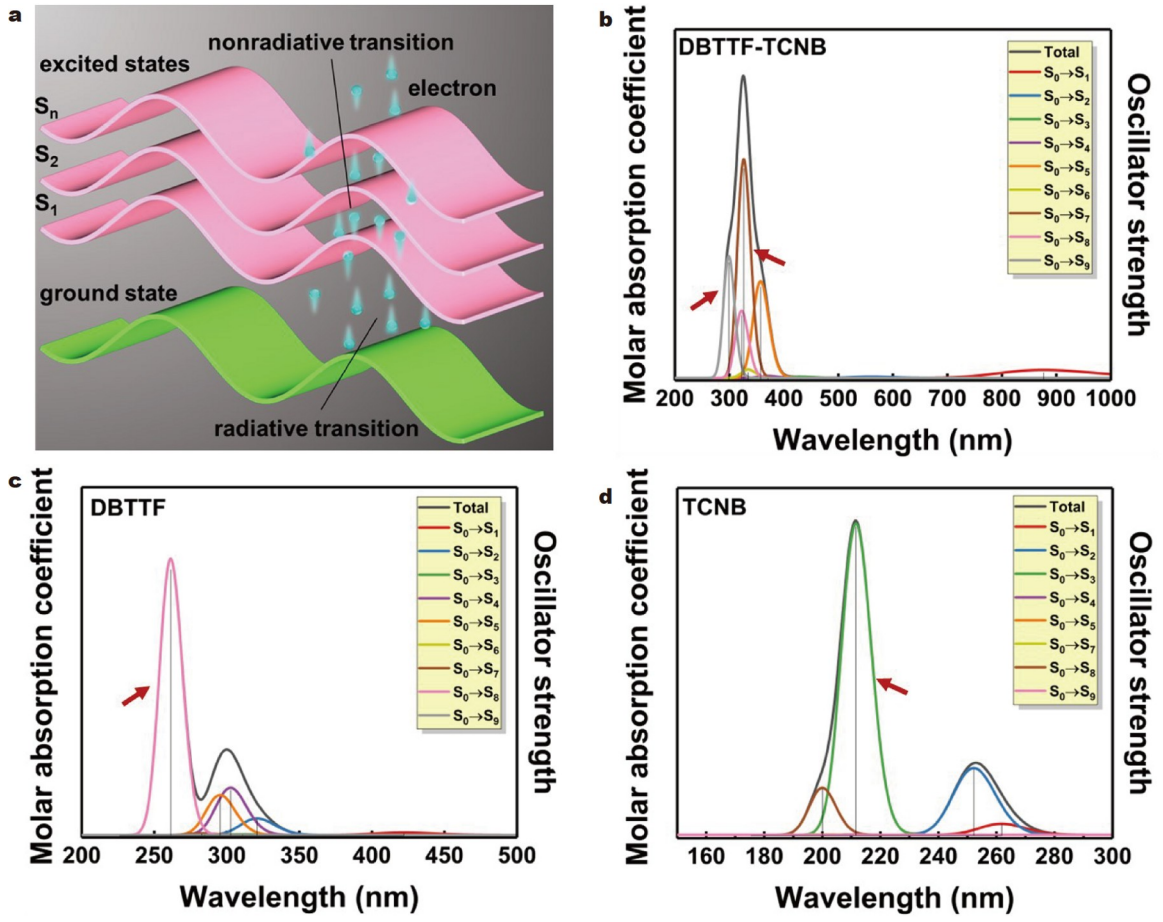

Figure 1 Schematic of nonradiative and radiative transitions and simulated UV-Vis spectra. (a) Schematic of transitions between the ground and excited states; simulated UV-Vis spectra of (b) DBTTF-TCNB, (c) DBTTF and (d) TCNB.

analyze the CT processes of transitions between the ground and different excited states when the organic cocrystal system is excited. In addition, we investigate the backhaul processes from different excited states to S_1 state.

To perform this research, an organic cocrystal is selected as a representative system. In this way, the first PTC cocrystal—dibenzotetrathiafulvalene-tetracyanobenzene (DBTTF-TCNB) [7]—is definitely the best choice. Thus, the DBTTF-TCNB cocrystal and the corresponding single crystals, DBTTF and TCNB, are selected as research objects to obtain some rules and results of the PTC property.

EXPERIMENTAL SECTION

As abovementioned, the CT interaction between the donor and the acceptor is our research emphasis. We used the quantum chemistry program package Gaussian 16 [36] to calculate the ground and some different excited states. The time-dependent DFT (TD-DFT) [37], a popular method that achieves a good balance between accuracy and time consumption, was applied for the calculation of the excited states. For the calculation of the ground state, the B3LYP functional [38–40] was used because the system that used this functional had the lowest energy among several test systems. In addition, in the calculation of excited states, the PBE38 functional [41] was applied because the simulated spectrum of the system that used this functional was the closest to the experimental one [7] among several test systems. Related tests can be seen in Fig. S1a, b. To better describe the weak interaction, all calculations were added with the D3 dispersion correction with BJ-damping [41,42]. Besides the basis set def2-SVP [43,44] used in the functional selection of the ground state's calculation, the rest of the calculations used the basis set def-TZVP [45].

To process these result files, Multiwfn [46] was used to obtain a better description of CT interaction from different theoretical perspectives. Herein, we mainly used the main function 5, 11, and 18 [46]. Also, in the main function 18, subfunctions 1 [47], 8 [46],13 [46], 15 [46], and 16 [48] were used.

The crystal structures were all downloaded from Cambridge Crystallographic Data Centre (CCDC; DBTTF-TCNB: 1827246 [7]; DBTTF: 696271 [49]; TCNB: 1580510 [50]).

As these crystal structures were obtained using an X-ray single-crystal diffractometer, all nonhydrogen atoms were accurately calibrated. Therefore, only hydrogen atoms were optimized, and all nonhydrogen atoms were frozen in the optimization process.

The absorption range of the actual experimental spectrum usually starts at 200–300 nm. Calculating too many excited states easily produces errors caused by intersystem crossing. Thus, considering the two factors, we studied nine excited states by TD-DFT calculation.

Finally, GaussView 6 [51] was used to visualize the molecular structure. In addition, Visual molecular dynamics (VMD) [52]

was used to process data that came from Multiwfn [46] and visualize these data.

RESULTS AND DISCUSSION

Contribution analysis of excited states

From other related experimental data [7], the absorption ranges of cocrystals are always wider than those of single crystals, which might correspond to the higher PTC efficiency of the cocrystal. Comparing Fig. 1b–d, it is found that the DBTTF-TCNB cocrystal system has a great proportion of higher excited states in the transition from the ground to different excited states. In this excitation process, the DBTTF-TCNB cocrystal system mainly transitions from S_0 state to S_7 state. However, some transitions also occur in S_0 state to S_9 or S_8 state. As for single-crystal systems, the DBTTF single-crystal system primarily transitions from S_0 state to S_8 state and that of TCNB primarily from S_0 state to S_3 state. Detailed values of the transition parameters of the three systems from the ground to different excited states are listed in Tables S1–S3. Among these, the minimum excitation energy for the transition from the ground state to S_1 state corresponds to the maximum absorption wavelength, which is a significant factor affecting the PTC efficiency. In general, the smaller the value of this minimum excitation energy, the larger the maximum absorption wavelength, the wider the absorption width, and the system may have a higher PTC efficiency. The three systems in this paper conform to this rule.

The results from previous work [7] exhibit that the absorption range of the DBTTF-TCNB cocrystal is the widest, followed by the DBTTF single crystal and the TCNB single crystal. Our calculation results are qualitatively consistent with the reported experimental result. This can confirm the rationality of our calculational method and make our inference more convincing. Getting back to our research system, fluorescence emission, which is a radiative transition, is the main approach for releasing energy in the process of de-excitation. Moreover, releasing energy in the form of heat, which belongs to the nonradiative transition, is a competitive relationship with the former. Thus, the greater the proportion of transition from the ground state to a higher excited state, the greater the proportion of backhaul from a higher excited state to S_1 state in the form of nonradiative transition in the de-excitation process, and more heat would be released.

In Tables S1–S3, the oscillator strength and its contribution to the total absorption of different transitions of the three systems are given. From these data, the TCNB system's proportion of higher excited states is small. This results in less nonradiative transition occurring and low PTC efficiency. Fortunately, the DBTTF system's transition is mainly from S_0 state to S_8 state, and the proportion reaches 71.71%. This is already a high proportion for this research, calculating only nine excited states. For the DBTTF-TCNB system, by contrast, its proportion is quite small (only 12.81%). However, the DBTTF-TCNB system's proportions of S_0 state to S_7 state transition and S_0 state to S_9 state transition are large, 41.64% and 23.16%, respectively. In particular, the S_0 state to S_9 state transition, the highest excited state in our research, accounts for 23.16%. This means that a great deal of nonradiative transition occurs during the de-excitation process, releasing a mass of heat at the macrolevel. This also explains the high PTC efficiency of the DBTTF-TCNB cocrystal.

In the actual de-excitation process, the system may also release energy in the form of phosphorescence emission, which requires the transitions between the triplet states. We mainly studied the theory of PTC efficiency based on Kasha's rule. To simplify the research object, the processes between triplet states are ignored. However, similarly, if the proportion that the ground state transitions to a high excited state is high, the probability of the conversion between singlet and triplet states would also be high in the backhaul process, and the energy will still be released in the form of thermal energy.

From Fig. 1b–d, there is a noticeable redshift in the simulated ultraviolet-visible (UV-Vis) spectrum of the cocrystal compared with its component single crystals. This is an interesting phenomenon, and its mechanism may be relative to the CT. We speculated that the energy required for the electron transition decreases after the CT completely occurs during the cocrystal process, leading to the redshift. Because several transitions in 300–400 nm substantially contribute to the total spectrum, the redshift could be mainly centered in this range, and there is obvious CT in these transitions. Thus, we next investigated the CT between the ground and excited states.

CT between the ground and excited states

The excitation process is ultimately attributable to electron excitation. Thus, we investigated the change in the hole and electron during the excitation process. It should be mentioned that the hole is the region where the excited electron leaves, and the electron is the region where the excited electron reaches.

Table 1 lists some basis parameters of the nine excitation processes, and their meanings and formulas are given in the Supplementary information. These parameters can be used to preliminarily examine the electron excitation characteristic. Except for the S_0 state to S_3 state transition, all *D*-indexes of the other transitions are large, demonstrating that the distance between the hole centroid and the electron centroid is relatively far. This phenomenon should be attributed to the CT excitation and accords with the common formation mechanism of cocrystals.

Our main point of interest is how to make as many electrons as possible transition from the ground state to a higher excited state. Thus, the research emphasis should be transferred to the S_0 state to S_7, S_8, and S_9 state transitions. Among these three transitions of the DBTTF-TCNB system, the proportion of S_0 state to S_7 state transition is the greatest, and that of S_0 state to S_8 state transition is the smallest. Comparing the positive or negative of $\Delta\sigma$ indexes, only the S_0 state to S_8 state transition has a positive value, meaning a substantially widely distributed electron. It might be less likely to occur or have a low probability of occurrence, causing a small proportion of this transition. In addition, comparing the *t* indexes, the S_0 state to S_7 state transition has the largest value, meaning a largest degree of separation between the hole and electron. Given the CT mechanism, this might be the best condition for electron excitation. Thus, this transition is most likely to occur, which corresponds to a great proportion.

The distribution, centroid, and overlapping extent of hole and electron are shown in Fig. S2. In Fig. S2a, b, the electron distributes in the acceptor—TCNB—and the hole distributes in the donor—DBTTF—in the S_0 state to S_1, S_2, S_4, S_5, S_6, and S_9 state transitions, which agrees with the theory of CT excitation in the cocrystal structure. However, other transitions seem not to be

Table 1 Basis parameters of the nine excitation processes of the DBTTF-TCNB system

Transition	S_r (a.u.)[a]	D (Å)[b]	$\Delta\sigma$ (Å)[c]	H (Å)[d]	t (Å)[e]	HDI[f]	EDI[g]	E_{coul} (eV)[h]
$S_0 \rightarrow S_1$	0.13258	4.712	−0.192	2.792	2.750	6.69	7.88	3.142716
$S_0 \rightarrow S_2$	0.12896	4.722	−0.519	2.627	2.971	6.69	8.57	3.124395
$S_0 \rightarrow S_3$	0.55640	0.284	0.170	2.883	−1.867	6.89	5.87	5.056052
$S_0 \rightarrow S_4$	0.15171	4.609	−1.221	3.308	2.157	5.48	7.88	3.133251
$S_0 \rightarrow S_5$	0.19819	3.824	−0.953	3.174	1.881	6.34	7.88	3.280402
$S_0 \rightarrow S_6$	0.17494	6.055	−1.064	3.248	3.489	6.33	7.83	2.713228
$S_0 \rightarrow S_7$	0.44477	3.871	−0.625	2.600	2.079	6.60	8.32	3.763427
$S_0 \rightarrow S_8$	0.51208	3.339	0.181	2.928	1.039	6.80	7.97	4.080016
$S_0 \rightarrow S_9$	0.25017	4.296	−1.101	3.344	1.874	5.45	8.26	3.226546

a) S_r: the overlapping extent of hole and electron; b) D: the distance between centroid of hole and electron; c) $\Delta\sigma$: the overall difference; d) H: the overall measure; e) t: the separation degree of hole and electron in CT direction; f) HDI: hole delocalization index; g) EDI: electron delocalization index; h) E_{coul}: the coulomb attraction energy between hole and electron, or exciton binding energy.

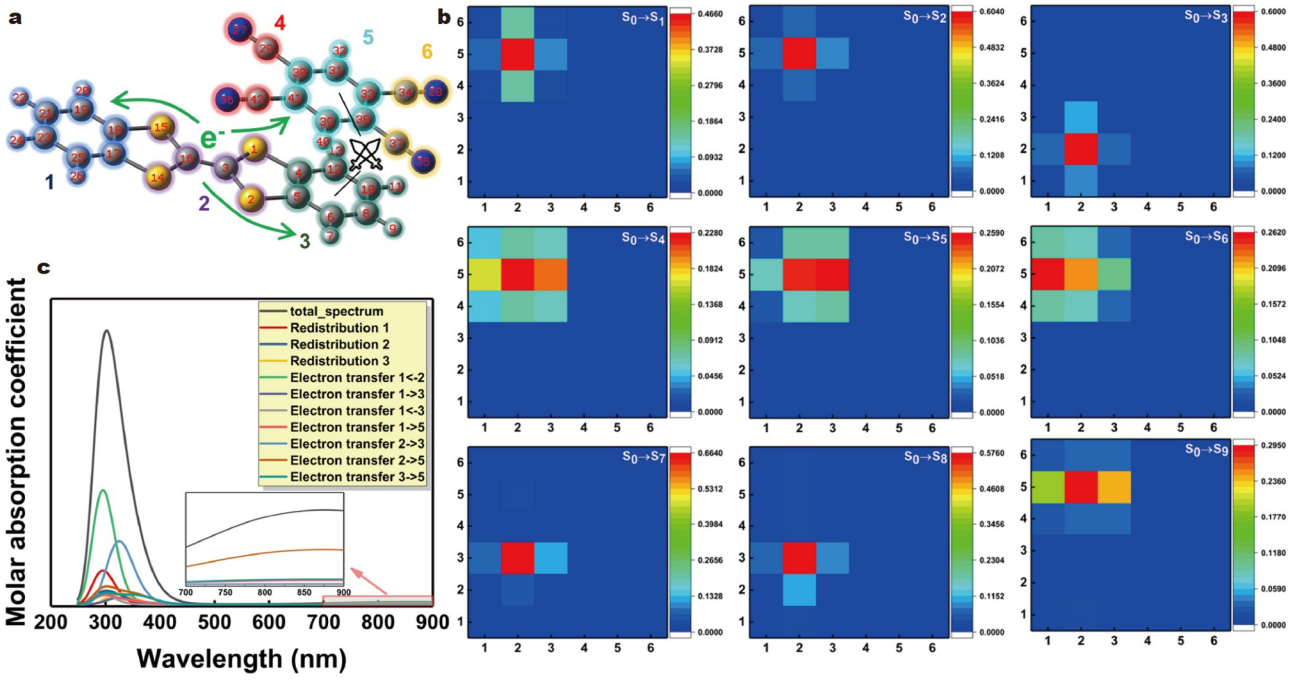

Figure 2 Molecular structure and CT between six fragments. (a) Molecular structure of the DBTTF-TCNB cocrystal and six divided fragments; (b) CT matrixes of six divided fragments from S_0 state to nine different excited states; (c) CT spectrum and its main fragment contribution to total spectrum.

conventional CT excitation, such as S_0 state to S_3 state, which looks like localized excitation. In addition, the D index of this transition is the smallest, which accords with the characteristic of localized excitation. The S_0 state to S_7 and S_8 state transitions are more like the CT excitation within the donor DBTTF.

In Fig. 2a, the donor DBTTF and the acceptor TCNB were divided into three fragments to quantitatively research the CT excitation. The amount of the CT between fragments was calculated by the interfragment CT (IFCT) method in Multiwfn [46,53] (see Table S4 for detailed quantitative values). These values determine how the charge is transferred between different fragments and the specific amount of the transferred charge.

In Fig. 2b, the excitation types of S_0 state to S_1 and S_2 states are similar, and those of S_0 to the S_4–S_6 and S_9 states are similar. The type of S_0 state to S_7 state is similar to that of S_0 state to S_8 state. Among the nine transitions of the DBTTF-TCNB system, the proportion of S_0 state to S_7 state is the greatest, reaching 41.64%, followed by S_0 state to S_9 state (23.16%), S_0 state to S_5 state (18.40%), and S_0 state to S_8 state (12.81%).

Next, focusing on S_0 state to S_7 state, it should be CT excitation because 83.086% is CT excitation and 16.914% is localized excitation, as shown in Table S4. In the CT matrix of S_0 to S_7 state, the CT excitation mainly takes place in the transfer from fragment 2 to 3 and rarely takes place in the transfer from fragment 2 to 5. Moreover, localized excitation might take place within fragment 3 itself. As a whole, the excitation mostly occurs within the donor DBTTF itself. Although some occur in the transfer from fragment 2 to 5, it is very little. Providing sufficient external energy to excite the DBTTF-TCNB system, it has the greatest proportion of S_0 state to S_7 state transition. It shows that this excitation type is suitable for this system. Alternatively, the S_0 state to S_8 state transition is similar to this excitation: its

proportion is also large. As previously stated, the excitation from S_0 to S_7 state mainly occurs within the donor DBTTF and comprises the CT excitation from fragment 2 to 3 and the localized excitation of fragment 3 itself. As for S_0 to S_9 state, it is obviously the CT excitation that occurs in the transfer from the donor DBTTF to fragment 5.

To occur as much nonradiative transition as possible in the backhaul process, as many transitions from the ground state to higher excited state as possible in the excitation process are needed. Considering this research system—DBTTF-TCNB—as an example, the greatest proportion of S_0 state to S_7 state transition might be ascribed to the CT excitation occurring in the donor DBTTF and a small amount of localized excitation. If the electron is excited in this way, the distance it travels is small; therefore, the system might be easily excited in this way. Although the great proportion of S_0 state to S_7 state transition is one of the reasons for the high PTC efficiency, the contribution of S_0 state to S_9 state transition cannot be ignored. In addition, we expect that the proportion of S_0 state to S_9 state transition can be enhanced. The reason for S_0 state to S_9 state might be the strong electron-withdrawing property of fragment 5, which results in the electron transfer from the donor DBTTF, namely, fragments 1–3, to fragment 5, leading to the CT excitation.

Analyzing the S_0 state to S_7 and S_9 states transitions, the reason for S_0 state to S_7 state might be the electron-withdrawing property of fragment 3, causing CT excitation that occurs within donor DBTTF and localized excitation of fragment 3 itself. Furthermore, S_0 state to S_9 state might be the electron-withdrawing property of fragment 5, leading to the CT from three fragments of the donor DBTTF to fragment 5. Thus, we speculate a strategy of PTC cocrystal design, that is, introducing the electron-withdrawing groups into the donor and the acceptor and making them against each other, as shown in Fig. 2a. Although the excitation type of cocrystal is mostly CT excitation, the electron-withdrawing competition between the donor and the acceptor may make the CT excitation change a little bit, which would be introduced into some localized excitation. Herein, this CT excitation mixed with localized excitation pertains to the transition from the ground state to a higher excited state. Therefore, this might lead to the great proportion of higher excited state and make the cocrystal system have high PTC efficiency.

The CT spectrum in Fig. 2c displays a large contribution to the total spectrum that occurs within donor DBTTF in the small wavelength range, that is, high excitation energy or excitation interval corresponding to higher excited states. In addition, in the interval, the transfer process from fragment 2 to 3 corresponds to the results in Fig. 2b. As negative values cannot be shown in the CT matrix, the transfer process from fragment 2 to 1 is ignored in Fig. 2b. Nevertheless, Fig. 2c makes up for that and shows a significant contribution of the transfer from fragment 2 to 1 to the total spectrum. There is a large contribution of the transfer from fragment 2 to 5 in the large wavelength range corresponding to the lower excited states, and it also corresponds to the results in Fig. 2b. The action of fragment 2 is shown in Fig. 2c. Thus, one should be added to the previous strategy of the PTC cocrystal design, that is, introducing the electron-donating groups into the donor, as shown in Fig. 2a. Briefly, the PTC efficiency is improved from two aspects: the transfer between the donor and the acceptor that might broaden the absorption range and the transfer occurring within the donor that might induce a transition from the ground state to a higher excited state, which can increase the probability of nonradiative transition occurring.

The transition density from the ground state to nine different excited states is visualized in Fig. 3, for example, S_0 state to S_7 state, S_0 state to S_9 state, S_0 state to S_5 state and S_0 state to S_8 state, which have a large proportion and broad transition density distribution. Moreover, this is consistent with the previous results: all are CT excitations except the excitation from S_0 to S_3 state, which is localized excitation by comparing the increase and decrease of density. As for the S_0 state to S_7 state transition,

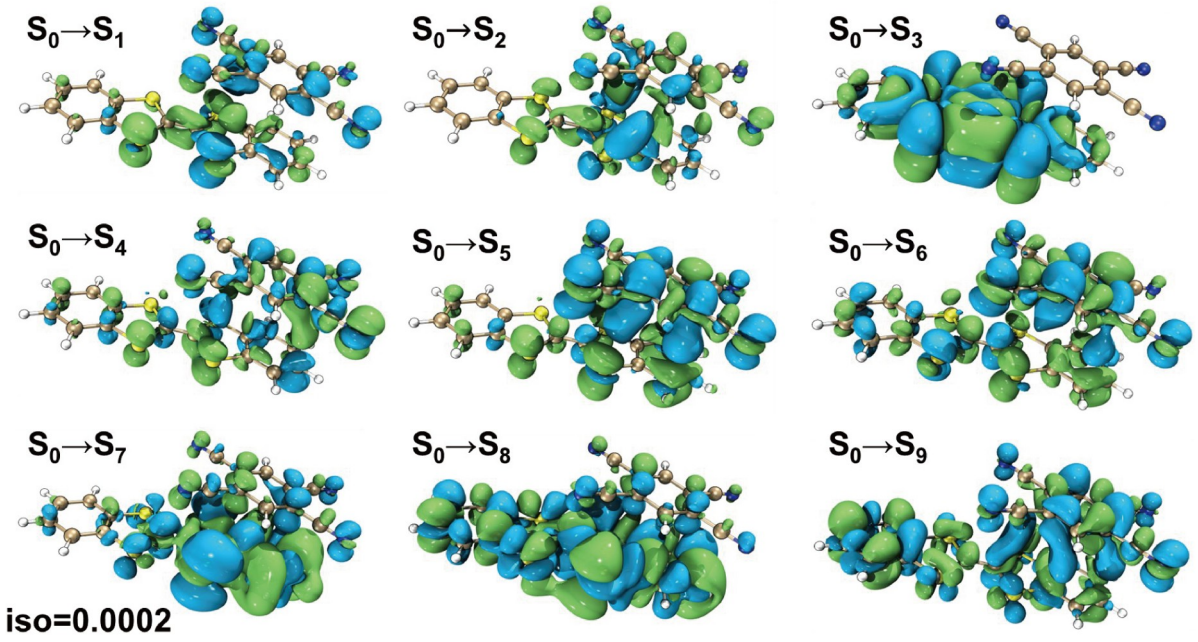

Figure 3 Transition densities from the ground state to nine different excited states. Green: positive; blue: negative.

the transition density is primarily distributed in fragments 2 and 3 of the donor, and a little is around the four cyano-groups in the acceptor. In Table S5, the S_0 state to S_7 state transition and S_0 state to S_9 state transition have large transition dipole moments, which exhibits the significant action of CT.

Orbital contribution to the excitation

In the TD-DFT method, electron excitation is usually expressed as transitions between numerous molecular orbitals. To examine the essence of excitation, the contribution of molecular orbital transition to electron excitation was explored. Fig. 4a shows the main contribution of the molecular orbital in different excitation processes, and its values are listed in Table S6. Except for the S_0 state to S_5 state transition and S_0 state to S_6 state transition, which have two kinds of orbital contribution, the others only have one. For the nine transitions, we are only interested in the two transitions: one is the S_0 state to S_7 state transition that has the greatest proportion, and the other is the S_0 state to this research's highest S_9 state transition. The orbital contribution of the first one is from the highest occupied molecular orbital (HOMO) to the lowest unoccupied molecular orbital (LUMO) + 3 orbital, whereas the second one is from HOMO-1 to LUMO + 1 orbital.

The orbital transition from HOMO to LUMO + 3 orbital plays a crucial role in the S_0 state to S_7 state excitation and mainly occurs within the donor DBTTF in Fig. 4b. As for the S_0 state to S_9 state excitation, the orbital transition from HOMO-1 to LUMO + 1 orbital mainly contributes to that, and it mainly occurs between the donor and the acceptor.

Electron density difference between different excited states and S_1 state

As previously stated, this research system is based on Kasha's rule, and therefore, the nonradiative transition occurs in the backhaul from other excited states to S_1 state. Fig. 5 illustrates the electron density difference between different states and S_1 state, in which green is positive and blue is negative. The electron density difference of every backhaul could illustrate the occurrence of the transition from excited states to S_1 state.

In Fig. 5, for the S_2 state to S_1 state backhaul, the variation occurs within the acceptor TCNB, demonstrating that electron transfer occurs here in this process. For the S_3 state to S_1 state backhaul, S_3 state might transfer electron from DBTTF to TCNB, which is similar to the CT in the cocrystal. Therefore, this also illustrates that this backhaul has a high probability of it occurring. Similarly, for the S_4 state to S_1 state, S_5 state to S_1 state, and S_6 state to S_1 state backhauls, the positive area is exactly where the electron-donating group is, and they are all with the possibility of occurrence. The S_7 state to S_1 state and S_8 state to S_1 state backhauls have the possibility of occurring because of the electron-withdrawing property of the acceptor TCNB. The S_9 state to S_1 state backhaul combines both mechanisms of the S_2 state to S_1 state backhaul and S_4 state to S_1 state backhaul, which also could occur in this process.

CONCLUSION

The first PTC cocrystal—DBTTF-TCNB—was examined by the DFT calculations. Our research emphasis is the transitions between the ground and excited states to explore its PTC

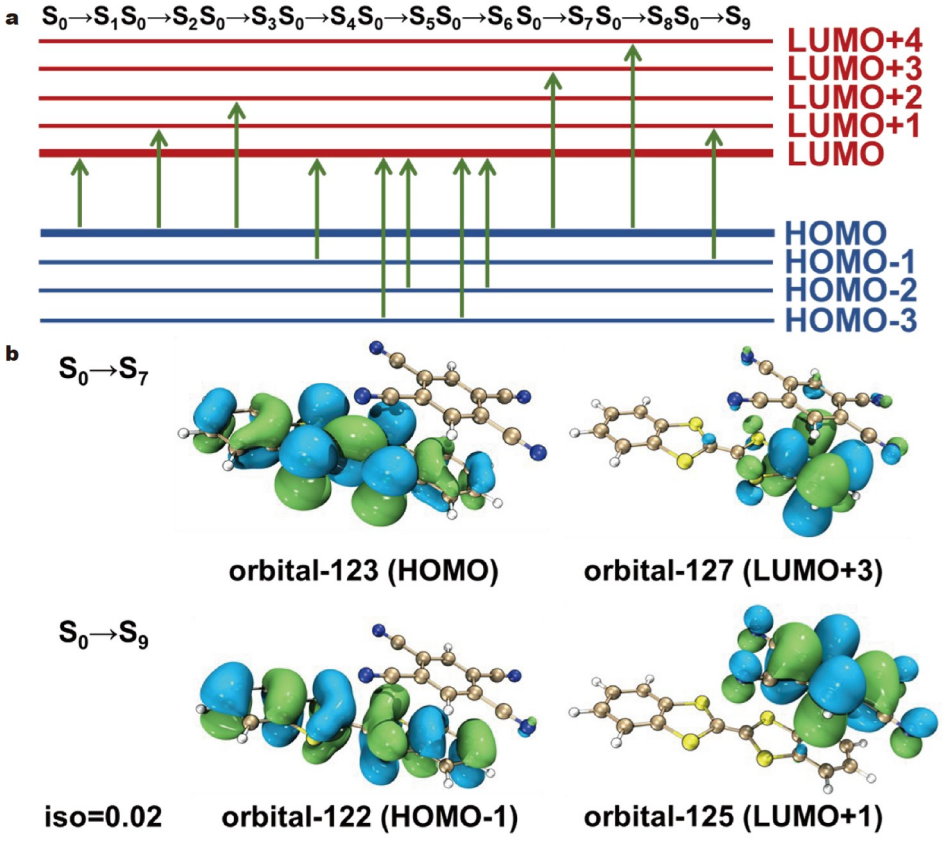

Figure 4 Orbital contributions and their molecular orbitals. (a) Main orbital contribution of transitions from the ground state to different excited states; (b) molecular orbitals of HOMO, LUMO + 3, HOMO-1 and LUMO + 1.

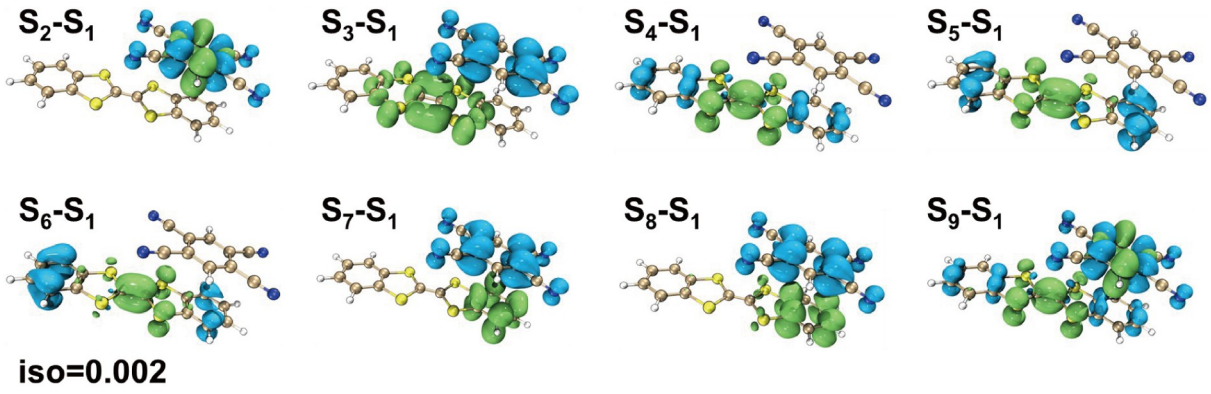

Figure 5 Electron density differences between different excited states and S_1 state.

mechanism. Based on Jablonski diagram and Kasha's rule, the occurrence of nonradiative transition could be explained by the different proportions of different excitations. The CT interaction plays a significant role in the cocrystal system. Thus, we conducted an exhaustive analysis of CT. In addition, several other methods were introduced to better explain this mechanism. The main results of this study are summarized below.

(1) In the de-excitation process, a great proportion of the transition from the ground state to a higher excited state might promote the occurrence of nonradiative transition and enhance the PTC efficiency. Compared with the DBTTF and TCNB systems, the greater proportion of the higher excitation of the DBTTF-TCNB could illustrate it.

(2) The DBTTF-TCNB molecular structure was divided into six fragments to explore the different actions of different regions. The electron-donating property of fragment 2 and the electron-withdrawing property of fragments 3 and 5 are the main motivating factors of the CT in the DBTTF-TCNB cocrystal. We also creatively came up with a strategy for the PTC cocrystal design.

(3) The orbital contribution of the transition shows the relationship between the molecular orbital and the excitation process. The molecular orbital of the key transitions and electron density difference support the possibility of excitation and backhaul, which further corroborates the previous results.

This paper used the TD-DFT method to examine the excitation and de-excitation processes and explain the reason for the higher PTC efficiency of the DBTTF-TCNB cocrystal than its component single crystals. Although there are several challenges and uncertainties in current research on the PTC mechanism of cocrystals, our findings may, to some extent, explain the relationship between the proportion of different excited states and PTC efficiency. We also explain the CT in the excitation process and the occurrence of nonradiative transition in the de-excitation process. Furthermore, we offer some suggestions for the molecular design of the PTC cocrystal. This paper obtains these theoretical calculation results based on the small-molecule system. Future work might expand the research model and consider some macroscopic external factors that affect the performance. Finally, it is expected that these results would offer some guidance and help for the application of the PTC cocrystal in innovative fields, such as photothermal imaging, biological application, and seawater desalination, from the perspective of quantum chemistry.

Received 31 August 2023; accepted 14 November 2023; published online 25 December 2023

1 Sun L, Wang Y, Yang F, *et al.* Cocrystal engineering: A collaborative strategy toward functional materials. Adv Mater, 2019, 31: 1902328
2 Dasari RR, Wang X, Wiscons RA, *et al.* Charge-transport properties of F_6 TNAP-based charge-transfer cocrystals. Adv Funct Mater, 2019, 29: 1904858
3 Sun Y, Lei Y, Dong H, *et al.* Solvatomechanical bending of organic charge transfer cocrystal. J Am Chem Soc, 2018, 140: 6186–6189
4 Wang Y, Wu H, Zhu W, *et al.* Cocrystal engineering: Toward solution-processed near-infrared 2D organic cocrystals for broadband photodetection. Angew Chem Int Ed, 2021, 60: 6344–6350
5 Wiscons RA, Goud NR, Damron JT, *et al.* Room-temperature ferroelectricity in an organic cocrystal. Angew Chem Int Ed, 2018, 57: 9044–9047
6 Chen YT, Zhuo MP, Wen X, *et al.* Organic photothermal cocrystals: Rational design, controlled synthesis, and advanced application. Adv Sci, 2023, 10: 2206830
7 Wang Y, Zhu W, Du W, *et al.* Cocrystals strategy towards materials for near-infrared photothermal conversion and imaging. Angew Chem Int Ed, 2018, 57: 3963–3967
8 Zhao YD, Han J, Chen Y, *et al.* Organic charge-transfer cocrystals toward large-area nanofiber membrane for photothermal conversion and imaging. ACS Nano, 2022, 16: 15000–15007
9 Shi P, Liu XX, Dai XL, *et al.* Near-infrared photothermal conversion properties of carbazole-based cocrystals with different degrees of charge transfer. CrystEngComm, 2022, 24: 4622–4628
10 Tian S, Bai H, Li S, *et al.* Water-soluble organic nanoparticles with programable intermolecular charge transfer for NIR-II photothermal anti-bacterial therapy. Angew Chem Int Ed, 2021, 60: 11758–11762
11 Xiang H, Yang Q, Gao Y, *et al.* Cocrystal strategy toward multifunctional 3D-printing scaffolds enables NIR-activated photonic osteosarcoma hyperthermia and enhanced bone defect regeneration. Adv Funct Mater, 2020, 30: 1909938
12 Ge W, Xu Y, Liu C, *et al.* Structural effect of NIR-II absorbing charge transfer complexes and its application on cysteine-depletion mediated ferroptosis and phototherapy. J Mater Chem B, 2021, 9: 8300–8307
13 Wu Q, Xia R, Wen H, *et al.* Nanoscale porphyrin assemblies based on charge-transfer strategy with enhanced red-shifted absorption. J Colloid Interface Sci, 2022, 627: 554–561
14 Ge W, Liu C, Xu Y, *et al.* Crystal engineering of ferrocene-based charge-transfer complexes for NIR-II photothermal therapy and ferroptosis. Chem Sci, 2022, 13: 9401–9409
15 Ou C, Na W, Ge W, *et al.* Biodegradable charge-transfer complexes for

glutathione depletion induced ferroptosis and NIR-II photoacoustic imaging guided cancer photothermal therapy. Angew Chem Int Ed, 2021, 60: 8157–8163
16 Wang D, Kan X, Wu C, *et al.* Charge transfer co-crystals based on donor–acceptor interactions for near-infrared photothermal conversion. Chem Commun, 2020, 56: 5223–5226
17 Tian S, Huang Z, Tan J, *et al.* Manipulating interfacial charge-transfer absorption of cocrystal absorber for efficient solar seawater desalination and water purification. ACS Energy Lett, 2020, 5: 2698–2705
18 Xu J, Chen Q, Li S, *et al.* Charge-transfer cocrystal *via* a persistent radical cation acceptor for efficient solar-thermal conversion. Angew Chem Int Ed, 2022, 61: e202202571
19 Chen YT, Wen X, He J, *et al.* Boosting near-infrared photothermal conversion by intermolecular interactions in isomeric cocrystals. ACS Appl Mater Interfaces, 2022, 14: 28781–28791
20 Chen YT, Chen W, He J, *et al.* Tailormade nonradiative rotation tuning of the near-infrared photothermal conversion in donor–acceptor cocrystals. J Phys Chem C, 2021, 125: 25462–25469
21 Chen W, Sun S, Huang G, *et al.* Unprecedented improvement of near-infrared photothermal conversion efficiency to 87.2% by ultrafast nonradiative decay of excited states of self-assembly cocrystal. J Phys Chem Lett, 2021, 12: 5796–5801
22 Hao XL, Guo JF, Zou LY, *et al.* Theoretical investigations on the photophysical properties for a series of symmetrical and asymmetrical carbazole-based cationic two-photon fluorescent probes: The magic of methyl groups. J Phys Chem C, 2019, 123: 9407–9419
23 Kim HM, Cho BR. Small-molecule two-photon probes for bioimaging applications. Chem Rev, 2015, 115: 5014–5055
24 Hao XL, Zhang L, Wang D, *et al.* Analyzing the effect of substituents on the photophysical properties of carbazole-based two-photon fluorescent probes for hypochlorite in mitochondria. J Phys Chem C, 2018, 122: 6273–6287
25 Chen Y, Ren A, Yang Z, *et al.* Theoretical study of radiative and nonradiative decay rates for $Cu(^{I})$ complexes with double heteroleptic ligands. Phys Chem Chem Phys, 2018, 20: 9419–9428
26 Zhao W, He Z, Tang BZ. Room-temperature phosphorescence from organic aggregates. Nat Rev Mater, 2020, 5: 869–885
27 Ye W, Ma H, Shi H, *et al.* Confining isolated chromophores for highly efficient blue phosphorescence. Nat Mater, 2021, 20: 1539–1544
28 Kohn W. Nobel lecture: Electronic structure of matter—wave functions and density functionals. Rev Mod Phys, 1999, 71: 1253–1266
29 Jones RO. Density functional theory: Its origins, rise to prominence, and future. Rev Mod Phys, 2015, 87: 897–923
30 Peverati R, Truhlar DG. Quest for a universal density functional: The accuracy of density functionals across a broad spectrum of databases in chemistry and physics. Phil Trans R Soc A, 2014, 372: 20120476
31 Sun J, Remsing RC, Zhang Y, *et al.* Accurate first-principles structures and energies of diversely bonded systems from an efficient density functional. Nat Chem, 2016, 8: 831–836
32 Medvedev MG, Bushmarinov IS, Sun J, *et al.* Density functional theory is straying from the path toward the exact functional. Science, 2017, 355: 49–52
33 Hammes-Schiffer S. A conundrum for density functional theory. Science, 2017, 355: 28–29
34 Jablonski A. Efficiency of anti-Stokes fluorescence in dyes. Nature, 1933, 131: 839–840
35 Kasha M. Characterization of electronic transitions in complex molecules. Discuss Faraday Soc, 1950, 9: 14–19
36 Frisch MJ, Trucks GW, Schlegel HB, *et al.* Gaussian 16, Revision C.01. Gaussian, Inc., Wallingford CT 2016
37 Gross EKU, Kohn W. Time-dependent density-functional theory. Adv Quantum Chem, 1990, 21: 255–291
38 Becke AD. Density-functional exchange-energy approximation with correct asymptotic behavior. Phys Rev A, 1988, 38: 3098–3100
39 Lee C, Yang W, Parr RG. Development of the Colle-Salvetti correlation-energy formula into a functional of the electron density. Phys Rev B, 1988, 37: 785–789
40 Becke AD. Density-functional thermochemistry. III. The role of exact exchange. J Chem Phys, 1993, 98: 5648–5652
41 Grimme S, Antony J, Ehrlich S, *et al.* A consistent and accurate *ab initio* parametrization of density functional dispersion correction (DFT-D) for the 94 elements H-Pu. J Chem Phys, 2010, 132: 154104
42 Grimme S, Ehrlich S, Goerigk L. Effect of the damping function in dispersion corrected density functional theory. J Comput Chem, 2011, 32: 1456–1465
43 Weigend F, Ahlrichs R. Balanced basis sets of split valence, triple zeta valence and quadruple zeta valence quality for H to Rn: Design and assessment of accuracy. Phys Chem Chem Phys, 2005, 7: 3297–3305
44 Weigend F. Accurate Coulomb-fitting basis sets for H to Rn. Phys Chem Chem Phys, 2006, 8: 1057–1065
45 Schäfer A, Huber C, Ahlrichs R. Fully optimized contracted Gaussian basis sets of triple zeta valence quality for atoms Li to Kr. J Chem Phys, 1994, 100: 5829–5835
46 Lu T, Chen F. Multiwfn: A multifunctional wavefunction analyzer. J Comput Chem, 2012, 33: 580–592
47 Liu Z, Lu T, Chen Q. An sp-hybridized all-carboatomic ring, cyclo[18]carbon: Electronic structure, electronic spectrum, and optical nonlinearity. Carbon, 2020, 165: 461–467
48 Liu Z, Wang X, Lu T, *et al.* Potential optical molecular switch: Lithium@cyclo[18]carbon complex transforming between two stable configurations. Carbon, 2022, 187: 78–85
49 Brillante A, Bilotti I, Della Valle RG, *et al.* The four polymorphic modifications of the semiconductor dibenzo-tetrathiafulvalene. CrystEngComm, 2008, 10: 1899–1909
50 Saraswatula VG, Sharada D, Saha BK. Stronger π···π interaction leads to a smaller thermal expansion in some charge transfer complexes. Cryst Growth Des, 2018, 18: 52–56
51 Dennington R, Keith TA, Millam JM. GaussView, Version 6.1.1. Semichem Inc., Shawnee Mission KS 2016
52 Humphrey W, Dalke A, Schulten K. VMD: Visual molecular dynamics. J Mol Graphics, 1996, 14: 33–38
53 Lu T. Multiwfn–A multifunctional wavefunction analyzer: software manual, Version 3.8(dev). Beijing Kein Research Center for Natural Sciences, 2022

Acknowledgements This work was supported by the Ministry of Science and Technology of China (2022YFA1204401), the National Natural Science Foundation of China (52121002 and U21A6002), and Tianjin Natural Science Foundation (20JCJQJC00300).

Author contributions Fu S designed the research protocol under the guidance of Zhang X. Fu S carried out theoretical calculations with the support from He D and Zhang X. Fu S wrote the paper under the guidance of Zhang X. All authors contributed to the general discussion.

Conflict of interest The authors declare that they have no conflict of interest.

Supplementary information Experimental details and supporting data are available in the online version of the paper.

Siyao Fu is a doctoral student at Tianjin Key Laboratory of Molecular Optoelectronic Sciences, School of Science, Tianjin University. His current research interest is quantum chemical calculation for organic cocrystals.

Xiaotao Zhang is a professor at Tianjin University. He received his PhD degree from the Institute of Chemistry, Chinese Academy of Sciences, in 2012 after he received his MSc degree (2007) from Zhejiang University. His research interest includes the design and synthesis of novel organic semiconductors and the fabrication and characterization of organic optoelectronic devices.

基于基态和激发态之间跃迁过程的DBTTF-TCNB共晶的光热转换机制

付思姚[1], 何旦[3], 张小涛[2*]

摘要 有机共晶, 由于其光热转换性质, 为光热成像、生物应用和海水淡化等诸多领域带来了希望和活力. 然而, 有机共晶的光热转换机制尤其缺少详细且深入的理论研究. 本研究使用含时密度泛函理论方法探索了激发和去激发过程, 并解释了DBTTF-TCNB共晶比其组分单晶具有更高光热转换效率的原因. 结果显示, 高激发态的高占比促进了非辐射跃迁的发生. 基于DBTTF-TCNB共晶中给电子基团和吸电子基团间的电荷转移结果, 我们发现给体和受体之间吸引电子的竞争可能会促进光热转换, 且给电子基团在共晶结构中也十分重要. 这些结果可为光热转换共晶的设计提供理论指导. 轨道贡献和电子密度差进一步证明了我们的结论. 因此, 本研究从量子化学的角度给光热共晶在创新领域的应用提供了理论依据.

